Neuron, Vol. 42, 411–421, May 13, 2004, Copyright ©2004 by Cell Press

Stoichiometry and Assembly of Olfactory Cyclic Nucleotide-Gated Channels

Jie Zheng[1] and William N. Zagotta*
Howard Hughes Medical Institute
Department of Physiology and Biophysics
Box 357290
University of Washington School of Medicine
Seattle, Washington 98195

Summary

Native ion channels are precisely tuned to their physiological role in neuronal signaling. This tuning frequently involves the controlled assembly of heteromeric channels comprising multiple types of subunits. Cyclic nucleotide-gated (CNG) channels of olfactory neurons are tetramers and require three types of subunits, CNGA2, CNGA4, and CNGB1b, to exhibit properties necessary for olfactory transduction. Using fluorescently tagged subunits and fluorescence resonance energy transfer (FRET), we find the subunit composition of heteromeric olfactory channels in the surface membrane is fixed, with 2:1:1 CNGA2:CNGA4:CNGB1b. Furthermore, when expressed individually with CNGA2, CNGA4 and CNGB1b subunits were still present in only a single copy and, when expressed alone, did not self-assemble. These results suggest that the precise assembly of heteromeric olfactory channels results from a mechanism where CNGA4 and CNGB1b subunits have a high affinity for CNGA2 but not for self-assembly, precluding more than one CNGA4 or CNGB1b subunit in the channel complex.

Introduction

In olfactory receptor neurons, the binding of odorant to surface receptors triggers an elevation in the intracellular concentration of cAMP. This, in turn, causes the opening of cation-selective CNG channels and depolarization of the neuron (Zufall and Munger, 2001). The olfactory CNG channels are specialized for their role in olfactory transduction (Matulef and Zagotta, 2003). They are tuned to open at physiological levels of cAMP and can detect even small changes in cAMP concentration resulting from the binding of odorant to its receptor. Their pore is permeable to both monovalent cations and to Ca^{2+}, another important second messenger in olfactory transduction. Finally, the channels are inhibited by Ca^{2+}/calmodulin (Chen and Yau, 1994; Trudeau and Zagotta, 2003). This Ca^{2+}-dependent negative feedback mechanism is thought to mediate olfactory adaptation (Kurahashi and Menini, 1997).

Many of the specialized properties of olfactory CNG channels result from their heteromeric composition. Like voltage-activated potassium channels, CNG channels are tetramers, composed of four subunits around a centrally located pore. Each subunit contains six transmembrane segments with intracellular amino- and carboxy-terminal domains that are accessible to cytosolic modulators (Matulef and Zagotta, 2003). The native olfactory CNG channels are composed of three types of subunits, CNGA2, CNGA4, and CNGB1b (Bonigk et al., 1999; Bradley et al., 1994, 2001; Dhallan et al., 1990; Goulding et al., 1992; Liman and Buck, 1994; Munger et al., 2001; Sautter et al., 1998). Whereas the CNGA2 subunit can form functional homomeric channels when heterologously expressed, the CNGA4 and CNGB1b subunits only produce functional channels as heteromers with CNGA2. However, when expressed with CNGA2, the CNGA4 and CNGB1b subunits confer a number of important physiological properties on the heteromeric channel including increased cAMP sensitivity, altered divalent permeation and blocking properties, and more rapid Ca^{2+}/calmodulin modulation (Table 1). These properties closely mirror the properties of native olfactory CNG channels (Bonigk et al., 1999; Bradley et al., 2001; Munger et al., 2001; Sautter et al., 1998).

CNG channels also play a fundamental role in phototransduction, closing in response to the decrease in cGMP concentration triggered by light absorption (Matulef and Zagotta, 2003). Rod photoreceptor CNG channels are composed of two types of subunits, CNGA1 (closely related to CNGA2) and CNGB1 (an alternatively spiced variant of CNGB1b) (Brown et al., 1995; Chen et al., 1993, 1994; Kaupp et al., 1989; Korschen et al., 1995). As in olfactory channels, the heteromeric composition of rod channels optimizes many of its properties for light detection (Bauer, 1996; Chen et al., 1994; Hsu and Molday, 1993; Shammat and Gordon, 1999). Surprisingly, the stoichiometry of rod channels has recently been shown to be three CNGA1 subunits and one CNGB1 subunit (Weitz et al., 2002; Zheng et al., 2002; Zhong et al., 2002).

While the assembly of accessory subunits in channels is generally precise, occurring with a fixed stoichiometry and arrangement in all channels, the assembly of pore-forming subunits can be either precise or random. Within a subfamily of voltage-dependent potassium channels, for example, the assembly appears to be nearly random, with all combinations and orientations produced (Jan and Jan, 1997). However, Ach receptor channels form with a precise stoichiometry and arrangement of four different subunit types in a pentamer (Kreienkamp et al., 1995; Sine et al., 1995). This precise assembly seems to be controlled, at least in part, by specific subunit interactions, with high-affinity interactions favoring assembly and low-affinity interactions precluding it (Li et al., 1992; Xu et al., 1995).

Here, we have determined the stoichiometry of heteromeric olfactory CNG channels at the surface membrane by using a fluorescence approach. The green fluorescent protein mutants, enhanced cyan fluorescent protein (eCFP), and enhanced yellow fluorescent protein

*Correspondence: zagotta@u.washington.edu
[1]Present address: University of California at Davis School of Medicine, Department of Physiology and Membrane Biology, One Shields Avenue, Davis, California 95616.

Table 1. Electrophysiological Properties of Homo- and Heteromeric Olfactory CNG Channels

Channel	Functional Expression	Activation by 5 μM cAMP	Block by Diltiazem	Ca^{2+}/Calmodulin Modulation
CNGA2	+	-	-	slow
CNGA4	-	NA	NA	NA
CNGB1b	-	NA	NA	NA
CNGA2+CNGA4	+	+	+	slow
CNGA2+CNGB1b	+	-	+	slow
CNGA2+CNGA4+CNGB1b	+	+	+	fast

Specifics are given in Figure 1 legend and Experimental Procedures.

(eYFP) were fused to the carboxyl terminus of each of the CNG channel subunits. To determine the stoichiometry of the heteromeric channels, we have performed two kinds of experiments: (1) we have determined the ratio of CNGA2:CNGA4 and CNGA2:CNGB1b subunits by directly quantifying the eCFP and eYFP fluorescence in the surface membrane, and (2) we have determined which subunits coassemble into the same channel complex by measuring the FRET between eCFP on one subunit and eYFP on another subunit. These experiments show that the assembly of heteromeric olfactory channels is precise. The CNGA4 and CNGB1b subunits were present in only a single copy when expressed individually with CNGA2 or when all three subunits are present. Furthermore, when expressed by themselves, CNGA4 and CNGB1b were present at low levels at the membrane surface but did not self-assemble. These results reveal the subunit stoichiometry of the heteromeric channels to be two CNGA2 to one CNGA4 to one CNGB1b subunit and suggest a plausible mechanism for their precise assembly.

Results and Discussion

Heteromeric channels were generated by coinjecting RNAs of the different subunits at defined ratios into *Xenopus* oocytes. Three different compositions of heteromeric olfactory channels were studied: CNGA2+CNGA4, CNGA2+CNGB1b, and CNGA2+CNGA4+CNGB1b, the presumed native composition. Each of these channel compositions has a unique signature of functional properties including activation by a low concentration of cAMP, block by L-*cis*-diltiazem, and modulation by Ca^{2+}/calmodulin (Table 1). Only channels containing CNGA4 are activated appreciably by 5 μM cAMP, only channels containing either CNGA4 or CNGB1b are blocked appreciably by 100 μM L-*cis*-diltiazem, and only channels containing both CNGA4 and CNGB1b are modulated rapidly by Ca^{2+}/calmodulin.

To determine the properties of the channels formed with each of the different RNA combinations, we recorded from the channels using the inside-out configuration of the patch-clamp technique. Each of the RNA combinations produced functional channels that displayed the signature properties expected for a nearly pure population of channels with the expected composition (Figure 1). In particular, all of the heteromeric channels were blocked appreciably by 100 μM L-*cis*-diltiazem, indicating that few, if any, CNGA2 homomeric channels were formed under these conditions (Figure 1A, green trace). In addition, only channels from the CNGA2+CNGA4 and CNGA2+CNGA4+CNGB1b combinations were activated appreciably by 5 μM cAMP, indicating the presence of the CNGA4 subunit (Figure 1A, red trace). And finally, virtually all of the channels from the CNGA2+CNGA4+CNGB1b combination, but not the others, were inhibited rapidly by Ca^{2+}/calmodulin (Figure 1B). These results are consistent with earlier work on the functional properties of these heteromeric channels (Bradley et al., 1994, 2001; Chen and Yau, 1994; Finn et al., 1998; Liman and Buck, 1994; Munger et al., 2001) and indicate that each of these combinations produced nearly a pure population of functional channels with the expected composition. From the Ca^{2+}/

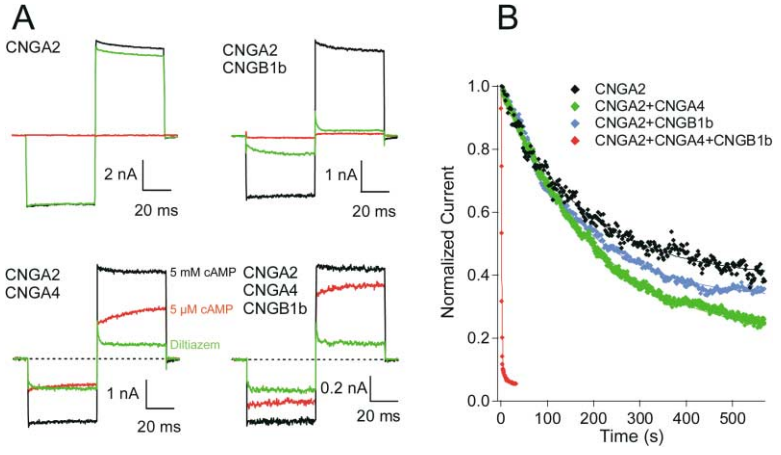

Figure 1. Electrophysiological Properties of Homo- and Heteromeric CNG Channels

(A) Inside-out patch currents in response to 5 μM cAMP (red) and to 5 mM cAMP without (black) and with 100 μM diltiazem (green).

(B) Time courses of current inhibition by Ca^{2+}/calmodulin. Smooth lines are single-exponential fits.

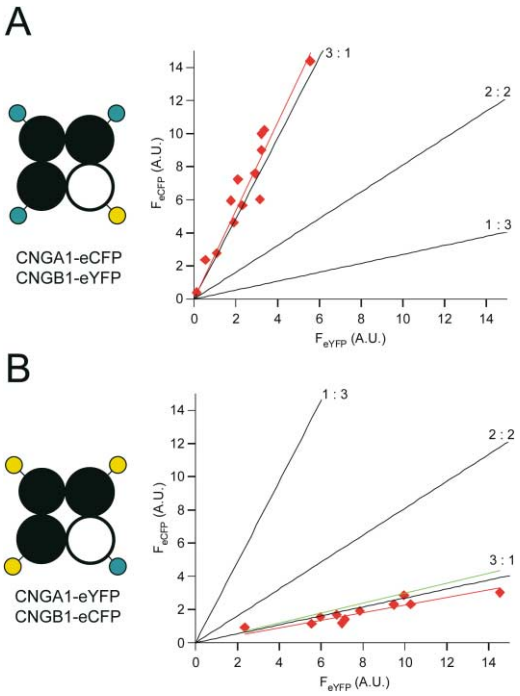

Figure 2. The FIR Measurements of the Subunit Ratio of CNGA1+CNGB1 Channels

Scatter plot of the eCFP intensity (F_{eCFP}) versus the eYFP intensity (F_{eYFP}) (in arbitrary units), measured from channels formed by (A) CNGA1-eCFP and CNGB1-eYFP subunits, or (B) CNGA1-eYFP and CNGB1-eCFP. Each point is from a different oocyte. The red lines are linear fits to each data set; the green lines represent the fluorescence intensity ratio after correction for the FRET-induced decrease in eCFP intensity; the black lines represent predicted fluorescence intensity ratios for channels of the indicated stoichiometry.

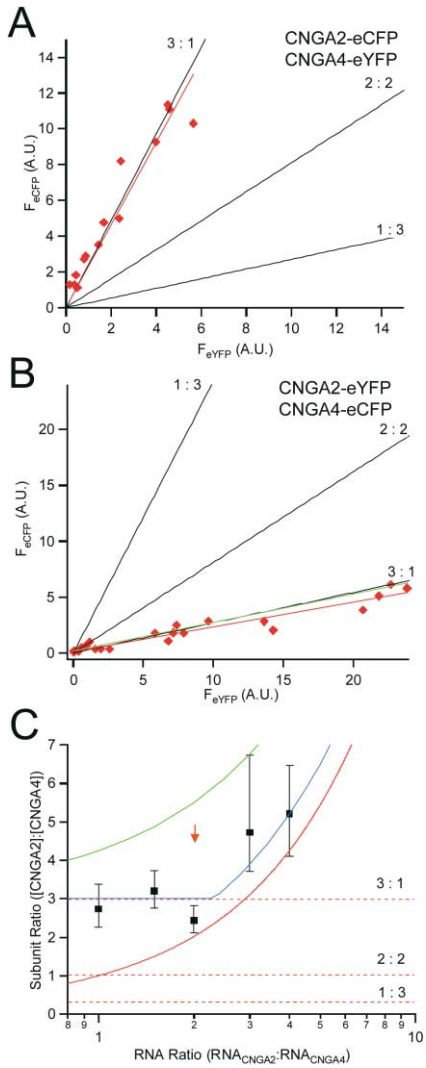

Figure 3. CNGA2+CNGA4 Channels Have a Subunit Ratio of 3:1

(A) Fluorescence intensity ratio plot of channels formed by CNGA2-eCFP and CNGA4-eYFP subunits.

(B) Fluorescence intensity ratio plot of channels formed by CNGA2-eYFP and CNGA4-eCFP subunits. The lines have the same meaning as in Figure 2.

(C) The subunit ratio as a function of the injected RNA ratio of CNGA2 and CNGA4. Error bars are 95% confidence limits. Horizontal lines represent channel stoichiometries of (from top) 3:1, 2:2, and 1:3, respectively. The smooth curves represent the expected subunit ratio for Model I (red), Model II (green), Model III (blue) (see Experimental Procedures). The arrow indicates the RNA ratio used elsewhere in this study.

calmodulin modulation data, for example, we estimate that at least 95% of the functional channels from the CNGA2+CNGA4+CNGB1b combination must contain all three subunits.

Fluorescence Intensity Ratio Method to Determine Stoichiometry

To determine the stoichiometry of heteromeric channels at the surface membrane, we have taken a fluorescence approach. The fluorescent proteins eCFP and eYFP were genetically attached to the carboxyl terminus of each of the CNG channel subunits. The fluorescence signal from fluorescently tagged channels expressed in *Xenopus* oocytes was measured using confocal microscopy. This approach has the advantage that fluorescence could be measured in intact cells from only the mature, properly assembled channels expressed in the surface membrane.

We first determined the ratio of different subunits in the surface membrane using a new method we have called fluorescence intensity ratio (FIR). With the FIR method, eCFP is fused to one subunit and eYFP is fused to another subunit. eCFP was excited with a 458 nm laser, and eYFP was excited with a 488 nm laser. The intensity of the eYFP fluorescence will then be proportional to the number of eYFP-tagged subunits, and the intensity of the eCFP fluorescence will be proportional to the number of eCFP-tagged subunits. The ratio of eYFP fluorescence to eCFP fluorescence will thus be proportional to the ratio of eYFP-tagged subunits to eCFP-tagged subunits. To correct for different excitation laser intensities and different extinction coefficients and quantum yields of the fluorophores, a similar measurement is made with eCFP and eYFP exchanged between subunits, putting eCFP on the subunit that used to have eYFP and vice versa. By comparing the two fluorescence ratios, one can calculate the correction factor to account for the different intensities of the indi-

vidual fluorophores and thereby calculate the ratio of subunits at the surface membrane (see Experimental Procedures).

Figure 2 illustrates an example of the use of this approach to determine the ratio of CNGA1 and CNGB1 subunits in the rod CNG channel. The fluorescence intensity of eCFP and eYFP was determined in oocytes expressing either CNGA1-eCFP+CNGB1-eYFP (Figure 2A) or CNGA1-eYFP+CNGB1-eCFP (Figure 2B). The eCFP intensity (F_{eCFP}) versus eYFP intensity (F_{eYFP}) is plotted from a number of oocytes with a range of fluorescence intensities and therefore expression levels. Also plotted are the predictions of CNGA1:CNGB1 ratios of 3:1, 2:2, and 1:3 (see Experimental Procedures). Clearly, the FIR method indicated a subunit ratio of 3:1, consistent with the stoichiometry of the rod channel determined from biochemical and FRET studies (Weitz et al., 2002; Zheng et al., 2002; Zhong et al., 2002).

One potential concern with the FIR method is the presence of FRET in these channel complexes. Indeed, eCFP and eYFP have previously been shown to function as a FRET pair (Miyawaki et al., 1997; Patterson et al., 2000), and FRET has been shown to occur in the CNGA1-eCFP+CNGB1-eYFP channels (Zheng et al., 2002). While this FRET would not affect the intensity of eYFP, the FRET acceptor, it is expected to attenuate the intensity of eCFP, the FRET donor. This is particularly a concern for CNGA1-eYFP+CNGB1-eCFP, where potentially three acceptors would be capable of quenching the eCFP fluorescence. To determine the extent of this quenching, we have determined the effective FRET efficiency by measuring the FRET ratio (Erickson et al., 2001; Zheng and Zagotta, 2003) (see Experimental Procedures). These calculations reveal that the fluorescence intensity of eCFP is only quenched ~24% in CNGA1-eYFP+CNGB1-eCFP channels. The correction of the data for this effect produced a minimal change in the graph (Figure 2B, green line) and does not affect the determination of the subunit ratio.

The native olfactory channel is composed of three types of subunits, CNGA2, CNGA4, and CNGB1b. To begin to determine the stoichiometry of these subunits and gain insights into the mechanism of assembly, we measured the ratio of CNGA2 and CNGA4 subunits for CNGA2+CNGA4 channels in the surface membrane (Figures 3A and 3B). Surprisingly, the CNGA2:CNGA4 ratio in CNGA2+CNGA4 channels was 3:1, just like CNGA1:CNGB1 in the rod channel. Previously, based on dimer studies, the stoichiometry of the CNGA2+CNGA4 channels was proposed to be 2:2 with an A2-A2-A4-A4 arrangement (Shapiro and Zagotta, 1998). While the CNGA2+CNGA4 channels do contain neighboring CNGA2 subunits as predicted, only a single copy of the CNGA4 subunit is present per channel, suggesting that the dimers were not incorporated as expected in the intact channel.

The CNGA2:CNGA4 ratio in the membrane was calculated from oocytes with different ratios of injected RNA. A subunit ratio of 3 was determined over a range of RNA ratios that have been shown previously to produce a functionally pure population of heteromeric CNGA2+CNGA4 channels (Figure 3C, the red arrow indicates the RNA ratio used elsewhere in this study; Shapiro and Zagotta, 2000). When higher RNA_{CNGA2}:RNA_{CNGA4} ratios were used, the subunit ratio CNGA2:CNGA4 in the membrane increased steeply above 3. This reflects the formation of homomeric CNGA2 channels at these high RNA ratios. The dependence of the subunit ratio on the RNA ratio is consistent with a model where all of the CNGA4 subunits preferentially assemble into CNGA2+CNGA4 channels with a stoichiometry of 3:1, and only excess CNGA2 subunits assemble into homomeric CNGA2 channels (Figure 3C, blue line; Model III, see Experimental Procedures). This model suggests that the CNGA4 subunits have a high affinity for CNGA2 subunits during assembly but cannot occur in more than a single copy

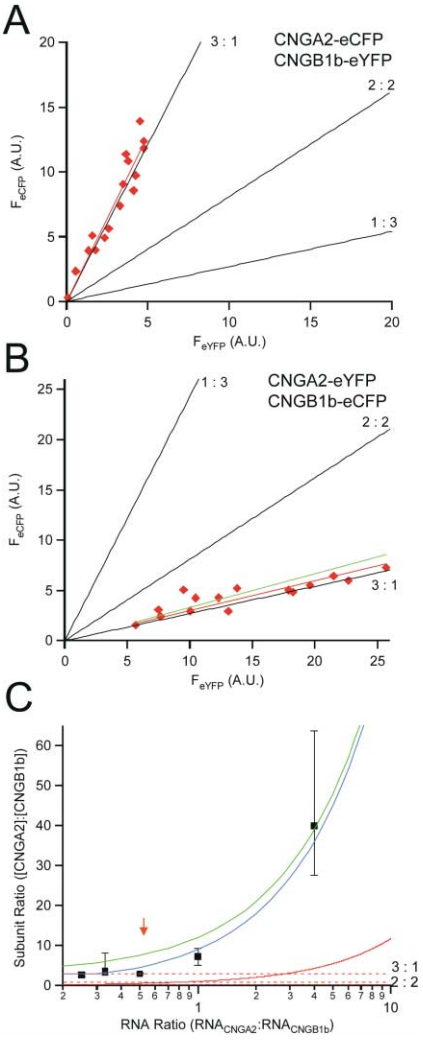

Figure 4. CNGA2+CNGB1b Channels Have a Subunit Ratio of 3:1

(A) Fluorescence intensity ratio plot of channels formed by CNGA2-eCFP and CNGB1b-eYFP subunits.

(B) Fluorescence intensity ratio plot of channels formed by CNGA2-eYFP and CNGB1b-eCFP subunits. The lines have the same meaning as in Figure 2.

(C) The subunit ratio as a function of the injected RNA ratio of CNGA2 and CNGB1b. Error bars are 95% confidence limits. Horizontal lines represent channel stoichiometries of (from top) 3:1, 2:2, and 1:3, respectively. The smooth curves represent the expected subunit ratio for Model I (red), Model II (green), Model III (blue) (see Experimental Procedures). The arrow indicates the RNA ratio used elsewhere in this study.

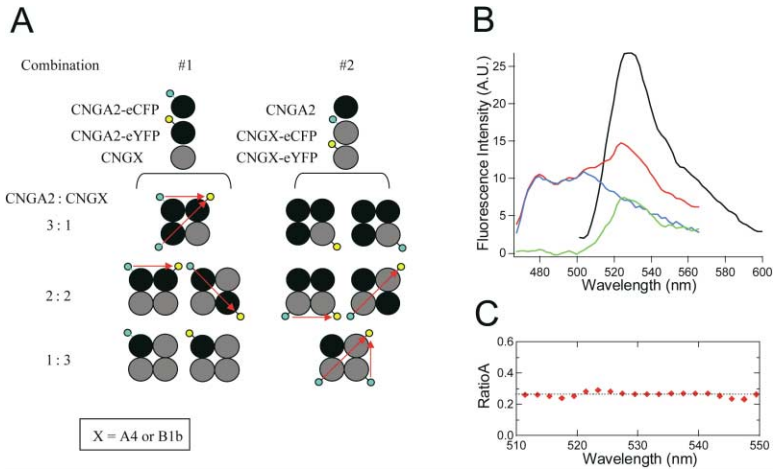

Figure 5. Determination of Channel Stoichiometry with FRET

(A) Diagram of the FRET experimental design. A red arrow indicates FRET between eCFP (cyan) and eYFP (yellow).

(B) Spectral quantification of the FRET efficiency. Emission spectra measured from an oocyte expressing CNGA2-eCFP, CNGA2-eYFP, and CNGB1b subunits are color-coded as follows: red, 458 nm excitation; black, 488 nm excitation (F_{488}); blue, standard eCFP emission spectrum; green, subtracted spectrum (difference between red and blue, F_{458}).

(C) RatioA measured over a range of wavelengths.

in the channels at the surface membrane. The data are inconsistent with other models assuming random assembly of CNGA2 and CNGA4 (Figure 3C, green and red lines; Models I and II, see Experimental Procedures). As for the CNGA1+CNGB1 channels, the calculated subunit ratio was not significantly altered by FRET, and the deduced stoichiometry is further supported by the FRET experiments discussed below.

We performed similar experiments to determine the ratio of CNGA2 and CNGB1b subunits for CNGA2+CNGB1b channels in the surface membrane (Figures 4A and 4B). As previously shown for the CNGA1+CNGB1 channels (Figure 2), the CNGA2:CNGB1b subunit ratio was also determined to be 3:1. This is not surprising, because the CNGA2 subunit is 70% similar to the CNGA1 subunit and the CNGB1b subunit is an amino-terminal alternatively spiced variant of CNGB1. A ratio of 3:1 was maintained over a range of RNA ratios that have been shown previously to produce a functionally pure population of heteromeric CNGA1+CNGB1 channels (Figure 4C; Shammat and Gordon, 1999). These data are also most consistent with a model where the CNGB1b subunit has a high affinity for CNGA2 subunits during assembly but cannot occur in more than a single copy in the channels at the surface membrane (Figure 3C, blue line; Model III).

FRET Determination of Stoichiometry

The above experiments indicate the ratio of subunits in the membrane, but they do not show conclusively the ratio of subunits in the channel. To determine the stoichiometry of the heteromeric channels more directly, we have used an approach based on FRET. FRET reports the proximity of two fluorophores (Clegg, 1992; Selvin, 1995). Light energy absorbed by a donor fluorophore is transferred to a nearby acceptor fluorophore, whose absorption spectrum overlaps the emission spectrum of the donor. The efficiency of energy transfer falls off with the sixth power of the distance between the donor and acceptor molecules, making FRET a sensitive reporter of proximity. The fluorescent proteins eCFP and eYFP have previously been shown to function as a FRET pair with a characteristic distance for 50% transfer efficiency (R_0) of approximately 50 Å (Miyawaki et al., 1997; Patterson et al., 2000). This distance makes them optimal for reporting the presence of two fluorescently tagged subunits in the same channel.

Using this approach, we could determine which subunit is present in two or more copies in intact heteromeric channels at the membrane surface. For channels composed of just two types of subunits, the experimental strategy is shown in Figure 5A. To test CNGA2, for example, we have coexpressed CNGA2-eCFP and CNGA2-eYFP, along with an untagged version of the other subunit that makes up the heteromeric channel (Figure 5A). The occurrence of FRET (red arrows) indicates the presence of CNGA2 in two or more copies in the channel. A similar experiment can be done for the other type of subunit to determine if it is present in two or more copies. Since the channel is known to be a

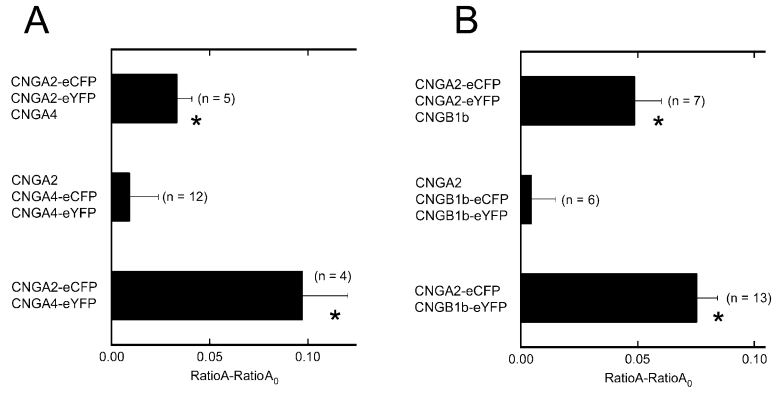

Figure 6. Both the CNGA2+CNGA4 Channel and the CNGA2+CNGB1b Channel Have a 3:1 Stoichiometry

The FRET efficiencies, expressed as the mean value of (RatioA − $RatioA_0$) and SEM, are shown for CNGA2+CNGA4 channels (A) and CNGA2+CNGB1b channels (B), with the number of oocytes given in parentheses. Asterisks indicate significant difference ($p < 0.05$).

tetramer (Liu et al., 1996; Varnum and Zagotta, 1996), these data are sufficient to establish the stoichiometry of the heteromeric channel. We have used this approach successfully for the rod CNGA1+CNGB1 channel (Zheng et al., 2002) where a stoichiometry of 3:1 was also obtained by the FIR method (Figure 2) and by biochemical methods (Weitz et al., 2002; Zhong et al., 2002).

We quantified FRET efficiency using a spectrum approach (Figure 5B; Clegg, 1992; Selvin, 1995; Zheng et al., 2002, 2003). Briefly, FRET was measured as emission of the acceptor (eYFP) during donor (eCFP) excitation with a 458 nm laser. The eYFP emission spectrum was extracted from the total spectrum (Figure 5B, red line) by subtracting the eCFP component using a scaled eCFP spectrum collected from control oocytes expressing only eCFP-tagged channels (CNGA2-eCFP) (Figure 5B, blue line). The ratio of the extracted spectrum (F458, green line) to the eYFP spectrum from the same oocyte with direct excitation with a 488 nm laser (F488, black line) was calculated as RatioA. RatioA was independent of wavelength (Figure 5C), confirming that the eCFP component was properly subtracted and we were operating in the linear range of the detector. The RatioA component due to direct excitation of eYFP by the 458 nm laser ($RatioA_0$) was measured directly from control oocytes expressing only eYFP-tagged channels (CNGA2-eYFP) and subtracted from RatioA, yielding a value ($RatioA - RatioA_0$) that was directly proportional to FRET efficiency.

We have first used FRET to determine the stoichiometry of CNGA2+CNGA4 channels (Figure 6A) and CNGA2+CNGB1b channels (Figure 6B). As expected, both heteromeric channels display significant ($p < 0.05$) FRET between CNGA2-eCFP and CNGA2-eYFP, indicating the occurrence of more than one copy of the CNGA2 subunit in the channel. In contrast, the CNGA4 and CNGB1b subunits did not exhibit a significant FRET signal in their respective channels. This is despite a robust eCFP and eYFP signal from these membranes. In addition, both CNGA4-eYFP and CNGB1b-eYFP received significant FRET excitation from CNGA2-eCFP ($p < 0.05$), indicating that the CNGA4 and CNGB1b subunits were assembled into heteromeric channels and capable of exhibiting FRET (Figure 6). These results indicate that CNGA4 and CNGB1b are present in only a single copy in CNGA2+CNGA4 and CNGA2+CNGB2b channels, respectively. Assuming the channels are tetramers, they must therefore have a stoichiometry of 3:1, as also suggested in the fluorescence intensity ratio experiments described above.

This approach can also be used to determine the stoichiometry of CNGA2+CNGA4+CNGB1b channels, the composition proposed for the native olfactory channel. For these experiments, we coexpressed all three types of subunits, with one subunit present in both an eCFP-tagged and an eYFP-tagged form (Figure 7A). As before, the occurrence of FRET indicates that subunit is present in two or more copies in the channel. Significant FRET was seen between CNGA2-eCFP and CNGA2-eYFP ($p < 0.05$), but not between CNGA4-eCFP and CNGA4-eYFP or between CNGB1b-eCFP and CNGB1b-eYFP (Figure 7B). However, FRET was observed between CNGA4-eYFP and CNGB1b-eCFP ($p < 0.05$),

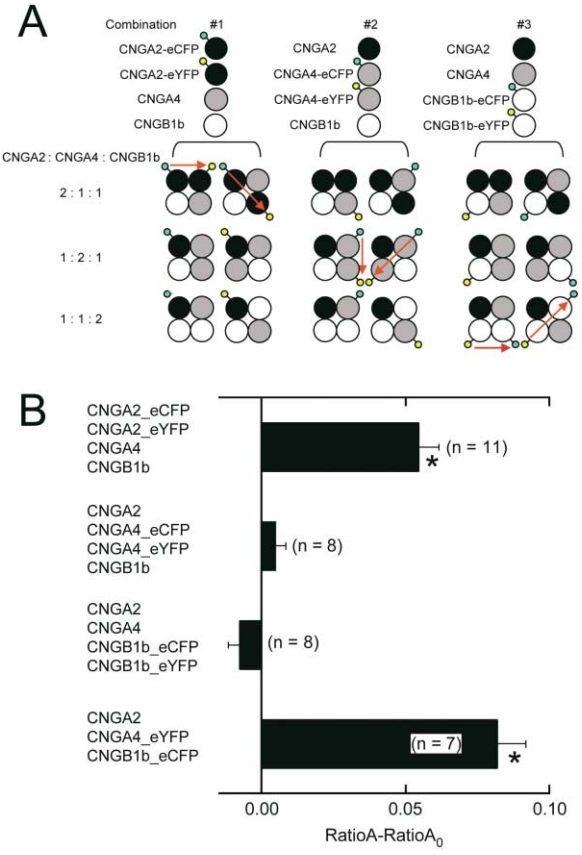

Figure 7. The CNGA2+CNGA4+CNGB1b Channel Has a 2:1:1 Stoichiometry

(A) Diagram of the FRET experimental design. A red arrow indicates FRET between eCFP (cyan) and eYFP (yellow).

(B) Mean values of ($RatioA - RatioA_0$) and SEM for each experiment, with the number of oocytes given in parentheses. Asterisks indicate significant difference ($p < 0.05$).

indicating that these subunits coassembled in the heteromeric channels. In fact, the rapid inhibition by calmodulin of nearly all of the current in CNGA2+CNGA4+CNGB1b channels (Figure 1C) strongly suggests that virtually all of the channels are composed of all three subunits. The absence of any detectable FRET signal between CNGA4 subunits and between CNGB1b subunits indicates that these subunits are rarely, if ever, present in more than a single copy each. These results, then, indicate the stoichiometry of the CNGA2+CNGA4+CNGB1b channels is 2:1:1 and is precisely controlled.

Mechanism of Precise Assembly of Olfactory Channels

What mechanism of assembly can account for this precision? One clue comes from our findings from varying the RNA ratios. These data were consistent with a mechanism where the CNGA4 and CNGB1b subunits both have a high affinity for CNGA2 subunits during assembly but cannot occur in more than a single copy in the channels at the surface membrane (Figures 3 and 4). This mechanism suggests that the CNGA4 and

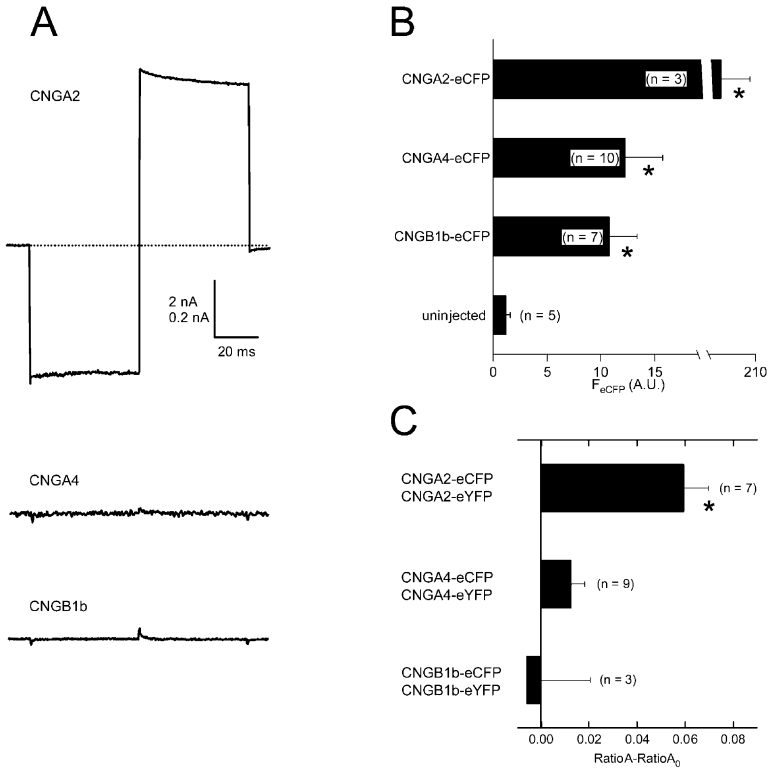

Figure 8. The CNGA4 Subunit and the CNGB1b Subunit Express at the Membrane Surface but Do Not Self-Assemble

(A) Inside-out patch currents from oocytes expressing the CNGA2, CNGA4, or CNGB1b subunit in response to 5 mM cAMP. Vertical scale bar equals 2 nA for the top panel and 0.2 nA for both middle and bottom panels.

(B) Mean fluorescence intensities and SEM measured from the surface membrane of oocytes expressing the eCFP-tagged subunits.

(C) FRET efficiency expressed as the mean values of (RatioA − $RatioA_0$) and SEM, with the number of measurements given in parentheses. Asterisks indicate significant difference ($p < 0.05$).

CNGB1b subunits cannot self-assemble. We tested this prediction by recording from oocytes that individually expressed fluorescently tagged CNGA2, CNGA4, or CNGB1b subunits. As seen previously, CNGA2 formed functional homomeric channels that produced large ionic currents in inside-out membrane patches (Figure 8A). In contrast, CNGA4 and CNGB1b did not produce functional homomeric channels. Interestingly, CNGA4-eCFP and CNGB1b-eCFP could be detected at low levels on the surface membrane (Figure 8B). The expression was approximately 5% of that seen for CNGA2-eCFP channels and was significantly ($p < 0.05$) above background fluorescence. These results suggest that the CNGA4 and CNGB1b subunits can indeed reach the membrane surface, albeit inefficiently.

We next used our FRET approach to determine if the CNA4 or CNGB1b subunits that reached the surface membrane were able to self-assemble. As expected, a significant FRET signal was observed in oocytes expressing only CNGA2 subunits ($p < 0.05$). Surprisingly, however, no FRET signal was present in oocytes expressing only CNGA4 or only CNGB1b (Figure 8C). For all of these oocytes, the eCFP and eYFP fluorescence was significantly above background, indicating the presence of both donor and acceptor subunits in the surface membrane. Furthermore, the lack of significant FRET for CNGA4 or CNGB1b could not be the result of lower expression of these subunits, as the method we employed expresses FRET as a ratio (RatioA − $RatioA_0$) that is insensitive to changes in the level of expression (Selvin, 1995; Zheng and Zagotta, 2003). These results, then, suggest that in the absence of CNGA2, the CNGA4 and CNGB1b subunits express at low levels as monomers in the surface membrane.

The results from this study suggest a plausible mechanism for the precise assembly of heteromeric olfactory channels with a stoichiometry of 2:1:1. In the abstract model in Figure 9, each subunit interacts with its neighbors in a head-to-tail arrangement during channel assembly with a 4-fold or pseudo 4-fold symmetry. The head-to-tail interactions between CNGA2 subunits are moderately favorable (indicated by gray shading in Figure 9A), allowing efficient homomeric channel formation. In contrast, because of differences in the head or tail structure, the CNGA4 and CNGB1b subunits do not self-assemble. Instead, these differences make the CNGA4 and CNGB1b subunits interact more favorably with the CNGA2 subunit (indicated by black shading in Figure 9A). Thus, CNGA2-CNGA4 and CNGA2-CNGB1b dimers might be expected to form first and then coassemble to produce the tetrameric channel (Figure 9B). The result is that virtually all of the CNGA4 and CNGB1b subunits are assembled into heteromeric channels and only excess CNGA2 subunits are available to form homomeric channels. This is the assembly model fit to the RNA ratio data in Figures 3 and 4 (blue line). If the CNGA4 and CNGB1b subunits can interact with CNGA2 using only their head or their tail, this could preclude inclusion of more than one copy of each subunit in the channel, but still allow one copy of both (Figure 9).

Such a model, while speculative, might have a foundation in the channel structure. While a member of the voltage-gated family of channels, CNG channels do not contain a tetramerization domain (T1) in their amino-terminal region (Varnum and Zagotta, 1997). Instead, extramembranous intersubunit interactions arise from amino-carboxy terminal interactions (Trudeau and Zagotta, 2002a, 2002b; Varnum and Zagotta, 1997; Zheng

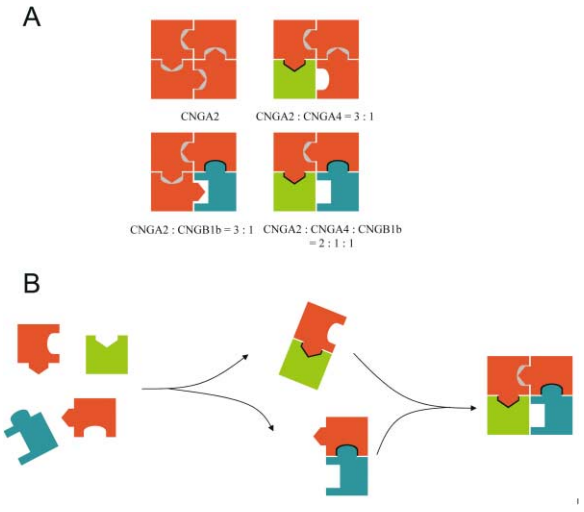

Figure 9. Assembly of Olfactory CNG Channel Subunits

Red, CNGA2; green, CNGA4; blue, CNGB1b. The model assumes that the CNGA2/CNGA4 interface and the CNGA2/CNGB1b interface exhibit higher affinities (black shading) than that of the CNGA2/CNGA2 interface (gray shading). Note that the CNGA4/CNGA4, CNGB1b/CNGB1b, and CNGA4/CNGB1b interfaces provide no interaction.

(A) Possible channel compositions.

(B) Mechanism of assembly.

et al., 2003) and carboxy-carboxy terminal interactions (Matulef and Zagotta, 2002; Zhong et al., 2002, 2003). These amino- and/or carboxy-terminal interacting domains could constitute the head and tail domains in Figure 9. In this regard, it is noteworthy that CNGA4 is nearly devoid of an intracellular amino-terminal region (Bradley et al., 1994; Liman and Buck, 1994). In addition, the amino-terminal region of CNGB1 has been shown to interact favorably with the distal carboxy-terminal region of CNGA1, but not its own carboxy-terminal region (Trudeau and Zagotta, 2002a, 2002b). These features might reduce CNGA4 and CNGB1b self-assembly. The distal carboxy-terminal region of CNGA1 has also been shown to self-associate into trimers, an interaction possibly involved in producing the 3:1 stoichiometry of rod CNGA1+CNGB1 channels (Zhong et al., 2003, 2002).

A more likely candidate, however, for the intersubunit interactions involved in assembly is the proximal carboxy-carboxy terminal interactions. The structural basis of these interactions was recently revealed with the elucidation of the high-resolution structure of the carboxy-terminal region of a hyperpolarization-activated cyclic nucleotide-modulated channel (HCN2) (Zagotta et al., 2003). HCN2 exhibits about 40% sequence similarity with the CNG channels in this region and is also modulated by cyclic nucleotides (Robinson and Siegelbaum, 2003). The carboxy-terminal region of each subunit contains a cyclic nucleotide binding domain and C-linker region that connects the cyclic nucleotide binding domain to the pore. Importantly, the carboxy-terminal region forms a 4-fold symmetric tetramerization domain on the intracellular face of the channel (Zagotta et al., 2003). The intersubunit interactions in this tetramerization domain occur almost exclusively between C-linkers, the first two α helices (A′ and B′) of one subunit interacting with the second two α helices (C′ and D′) of the neighboring subunit in a head-to-tail arrangement around the tetramer. These interactions between C-linkers could be the head-to-tail interactions hypothesized in Figure 9. CNGA4 and CNGB1b differ from CNGA2 at a number of positions involved in this interaction. Strikingly, a chimeric CNGA4 subunit, containing the C-linker region of CNGA1, was recently found to form functional homomeric channels (Zhou and Siegelbaum, 2001). These results provide a structural framework for understanding the mechanism for the precise assembly of olfactory CNG channels.

Experimental Procedures

Channel Constructs and Electrophysiology

The rat olfactory CNG channel subunits CNGA2 (formerly CNG2, olfactory α) (Dhallan et al., 1990), CNGA4 (formerly CNG5, olfactory β) (Bradley et al., 1994), and CNGB1b (Bonigk et al., 1999) were used in this study. eCFP (enhanced cyan fluorescent protein) and eYFP (enhanced yellow fluorescent protein) (Miyawaki et al., 1997) were genetically attached to the carboxy-terminal end of each subunit. The fluorescently tagged CNGA2 and CNGA4 subunits had a 21 amino acid linker (Q_8IEGRQ$_8$A) between the channel and fluorescent protein, and the fluorescently tagged CNGA2 had a deletion of amino acids 50–92 in the amino-terminal region. The eCFP and eYFP-tagged channels exhibited functional behaviors indistinguishable from those without fluorescence protein tags. All the constructs were made with a PCR-based method and confirmed with fluorescence-based DNA sequencing. These cDNAs were subcloned into a high expression vector that contained the untranslated sequence of the *Xenopus* β-globin gene (Liman et al., 1992). RNA for oocyte injections was made with the Message Machine kit (Ambion, Austin, TX), quantified with gel electrophoresis, and injected at the indicated ratios. The fluorescently tagged bovine rod CNG channel subunits CNGA1 and CNGB1, used here as positive controls, were made in a similar way and have been described previously (Zheng et al., 2002).

Xenopus oocytes were microinjected with a mixture of CNG channel RNAs and incubated for 3–7 days at 16°C prior to recording. RNA ratios of 2:1 for CNGA2+CNGA4, 1:2 for CNGA2+CNGB1b, and 2:1:4 for CNGA2+CNGA4+CNGB1b were used in all the experiments except those shown in Figures 3C and 4C. The RNA ratio of eCFP- to eYFP-tagged subunits of the same type was 2:1 to ensure that most of the eYFP-tagged subunits would coassemble with an eCFP-tagged subunit if possible. Incorporation of each subunit type was confirmed by fluorescence intensity from the fluorescent protein tags, as well as by electrophysiological properties.

Macroscopic ionic currents were recorded in the inside-out configuration of the patch-clamp technique using an Axopatch 200A patch-clamp amplifier (Axon Instruments, Foster City, CA) driven by PULSE software (HEKA) and digitized with an ITC-16 computer interface (Instrutech, Great Neck, NY). The patch membrane was held at 0 mV prior to 50 ms steps to −60 mV and +60 mV in the presence of the indicated solution. Leak currents in the absence of cyclic nucleotide were subtracted. The external (pipette) and internal (bath) solutions contained (in mM) 130 NaCl, 0.2 EDTA, 3 HEPES (pH 7.2). The internal solution, with cAMP (Sigma) added to a final concentration of up to 5 mM, was applied with an RSC-200 solution changer (Molecular Kinetics, Pullman, WA). L-*cis*-diltiazem (BIOMOL Research Laboratories) was applied at a final concentration of 100 μM in 5 mM cAMP solution. For the Ca^{2+}/calmodulin experiments in Figure 1B, the internal solution contained (in mM) 126 NaCl, 0.285 $CaCl_2$, 2 NTA-Na_2, 3 HEPES (pH 7.2), with 10 μM cGMP and 250 nM calmodulin (Calbiochem) added. The free Ca^{2+} concentration was calculated to be 30 μM.

Fluorescence Confocal Microscopy

Fluorescence emissions from eCFP- and/or eYFP-tagged channels were collected from the animal hemisphere of the oocyte with a

confocal microscope (Leica), using a 5× 0.15 NA objective and laser excitation of 458 nm and 488 nm, respectively. This configuration ensured that only fluorescence signals from the surface membrane were collected. When measuring spectra, the fluorescence intensity was quantified in 2 nm steps with a 5 nm window. A narrow range of PMT gain was used to ensure linearity, which was checked by calculating FRET efficiency in a wavelength range covering both strong and weak eYFP emission as described previously (Zheng et al., 2002). The level of background signal was estimated from a blank area of the same image and subtracted. For fluorescence intensity ratio measurements, a wider window of 30 nm was used to cover the peak emission for eCFP (475 to 505 nm) or eYFP (500 to 530 nm). The level of laser intensity and the PMT gain were kept the same for all experiments.

Quantification of FRET Efficiency with Fluorescence Emission Spectra

The spectrum-based approach to quantify FRET efficiency between eCFP and eYFP has been described previously (Zheng and Zagotta, 2003). This method has several advantages: (1) it allows accurate removal of contaminations due to donor emission and direct excitation of the acceptor, (2) it avoids errors arising from the transfer function of the recording system, variation in the quantum yield of the acceptor, or variation in the concentration of total fluorescence molecules, and (3) an internal check for system linearity is available (Clegg, 1992; Selvin, 1995). Briefly, two spectra were collected from each oocyte, one with 458 nm excitation and the other with 488 nm excitation. A scaled eCFP spectrum collected from control oocytes expressing eCFP-tagged channels was used to subtract eCFP emissions from the spectrum taken with 458 nm excitation, yielding an extracted eYFP emission spectrum, F_{458}. F_{458} had two components, one due to direct excitation of eYFP, F_{458}^{direct}, and one due to FRET, F_{458}^{FRET}. F_{458} was normalized by the total eYFP emission with 488 nm excitation, F_{488}. The resulted ratio, termed RatioA, can be expressed as

$$RatioA = \frac{F_{458}}{F_{488}} = \frac{F_{458}^{direct}}{F_{488}} + \frac{F_{458}^{FRET}}{F_{488}}. \quad (1)$$

The direct excitation component in RatioA, termed $RatioA_0$, was experimentally determined from oocytes expressing eYFP-tagged channels. The difference between RatioA and $RatioA_0$, (RatioA − $RatioA_0$), is directly proportional to FRET efficiency:

$$RatioA - RatioA_0 = \frac{F_{458}^{FRET}}{F_{488}}. \quad (2)$$

It is noted that (RatioA − $RatioA_0$) is independent of wavelength and provides a convenient internal check for linearity.

Fluorescence Intensity Ratio Analysis

Different subunit types were tagged with eCFP or eYFP and coexpressed in oocytes. The covalent linkage ensured that the intensity of fluorescence observed was proportional to the number of subunits of that type. When eCFP-tagged X subunits and eYFP-tagged Y subunits are coexpressed, the intensities of eCFP and eYFP can be calculated as

$$F_{eCFP} = C_1[X] \quad (3)$$

$$F_{eYFP} = C_2[Y], \quad (4)$$

in which F_{eCFP} and F_{eYFP} are eCFP and eYFP intensities with excitation at 458 nm and 488 nm, respectively; [X] and [Y] are the number of X-eCFP and Y-eYFP subunits; and C_1 and C_2 are constants reflecting the laser intensities, the system transfer function, the properties of the fluorophores, etc. The fluorescence intensity ratio is defined as

$$k_1 = \frac{F_{eCFP}}{F_{eYFP}} = \frac{C_1[X]}{C_2[Y]} = C \bullet \frac{[X]}{[Y]}, \quad (5)$$

in which C is a constant that equals C_1/C_2.

Similarly, coexpressing X-eYFP and Y-eCFP subunits yields a fluorescence intensity ratio

$$k_2 = \frac{F_{eCFP}}{F_{eYFP}} = \frac{C_1[Y]}{C_2[X]} = C/\left(\frac{[X]}{[Y]}\right). \quad (6)$$

From (5) and (6), both the subunit ratio and the constant C can be determined:

$$\frac{[X]}{[Y]} = \sqrt{\frac{k_1}{k_2}} \quad (7)$$

$$C = \sqrt{k_1 k_2}. \quad (8)$$

C was experimentally determined from the CNGA1+CNGB1 data in Figure 2. k_1 and k_2 were determined from the slope of linear fits to the data in Figures 2A and 2B, respectively, and C was calculated from equation 8. The same value of C was used for the CNGA2+CNGA4 and CNGA2+CNGB1b data in Figures 3 and 4. After C was experimentally determined, one can use equations 5 and 6 to calculate k_1 and k_2 for any given subunit ratio.

The FIR method assumes that the fluorescence emissions of eCFP and eYFP are independent. However, due to FRET, the observed eCFP intensities were artificially reduced in our experiments. The reduction of eCFP intensity is expected to be greatest in channels having multiple eYFP-tagged subunits next to an eCFP-tagged subunit. The eYFP intensity, measured with 488 nm excitation, should not be affected by FRET. To correct for this FRET-associated eCFP signal reduction, we calculated effective FRET efficiency values using the FRET ratio measurement (Erickson et al., 2001; Zheng et al., 2003). The ratio between RatioA and $RatioA_0$, termed FRET ratio or FR, is calculated as

$$FR = \frac{RatioA}{RatioA_0} = 1 + \frac{F_{458}^{FRET}}{F_{458}^{direct}}. \quad (9)$$

Like (RatioA − $RatioA_0$) discussed above, FR is also directly proportional to FRET efficiency. From FR the effective FRET efficiency, E_{eff}, was calculated as follows:

$$E_{eff} = \frac{\epsilon_{eYFP}}{\epsilon_{eCFP}}(FR - 1), \quad (10)$$

in which ϵ_{eCFP} and ϵ_{eYFP} are the molar extinction coefficient for eCFP and eYFP, respectively. Once E_{eff} was determined, the true eCFP intensity was calculated as

$$F_{eCFP\_true} = \frac{F_{eCFP\_observed}}{(1 - E_{eff})}. \quad (11)$$

Modeling of Channel Assembly with Varying Subunit Ratios

Three models were considered in this study to describe the dependence of the subunit ratio on the RNA ratio. In the first model, we assumed that when the two subunit species, X and Y, are coexpressed, they assemble randomly into all possible compositions according to the binomial distribution. In this simple case, the subunit ratio, [X]/[Y], is expected to depend on the RNA ratio, RNA_x/RNA_y, according to the following equation:

$$\frac{[X]}{[Y]} = \frac{4\gamma^4 + 12\gamma^3(1-\gamma) + 12\gamma^2(1-\gamma)^2 + 4\gamma(1-\gamma)^3}{4\gamma^3(1-\gamma) + 12\gamma^2(1-\gamma)^2 + 12\gamma(1-\gamma)^3 + 4(1-\gamma)^4}, \quad \text{(Model I)}$$

in which

$$\gamma = \left(g\frac{RNA_X}{RNA_Y}\right)/\left(g\frac{RNA_X}{RNA_Y} + 1\right),$$

where g is a correction factor that takes into account the difference in RNA expression efficiency and is the only free parameter in the models.

We applied the random assembly assumption to Model II as well. We further assumed that the Y subunit is present at most in a single copy, that is, only XXXX and XXXY channels are formed. The subunit ratio can be calculated as

$$\frac{[X]}{[Y]} = \frac{4\gamma^4 + 12\gamma^3(1-\gamma)}{4\gamma^3(1-\gamma)}. \qquad \text{(Model II)}$$

For Model III, we assumed that the X and Y subunits preferably assemble into XXXY channels; only the excess X subunits assemble into homomeric XXXX channels. Under these conditions, the subunit ratio can be calculated as follows:

$$\frac{[X]}{[Y]} = \begin{cases} 3 & \text{if} \quad \gamma \le 3/4 \\ \dfrac{\gamma}{1-\gamma} & \text{if} \quad \gamma > 3/4 \end{cases}. \qquad \text{(Model III)}$$

Acknowledgments

We thank the following people for the generous gift of DNA constructs: R. Reed for CNGA2 and CNGB1, K. Zinn for CNGA4, U.B. Kaupp for CNGB1b, R.Y. Tsein for eCFP and eYFP, and E. Liman for pGEMHE. We are grateful to Heidi Utsugi, Kevin Black, Gay Sheridan, and Shellee Cunnington for technical assistance, Greg Martin and Paulette Brunner of the Keck Imaging Center for help with confocal microscopy, Tsung-Yu Chen, Sharona E. Gordon, and Matthew C. Trudeau for comments on the manuscript, and members of the Zagotta lab for insightful discussions. This work was supported by the Howard Hughes Medical Institute and a grant from the National Eye Institute (EY10329) to W.N.Z.

Received: March 5, 2004
Revised: April 12, 2004
Accepted: April 14, 2004
Published: May 12, 2004

References

Bauer, P.J. (1996). Cyclic GMP-gated channels of bovine rod photoreceptors: affinity, density and stoichiometry of Ca(2+)-calmodulin binding sites. J. Physiol. *494*, 675–685.

Bonigk, W., Bradley, J., Muller, F., Sesti, F., Boekhoff, I., Ronnett, G.V., Kaupp, U.B., and Frings, S. (1999). The native rat olfactory cyclic nucleotide-gated channel is composed of three distinct subunits. J. Neurosci. *19*, 5332–5347.

Bradley, J., Li, J., Davidson, N., Lester, H.A., and Zinn, K. (1994). Heteromeric olfactory cyclic nucleotide-gated channels: a subunit that confers increased sensitivity to cAMP. Proc. Natl. Acad. Sci. USA *91*, 8890–8894.

Bradley, J., Reuter, D., and Frings, S. (2001). Facilitation of calmodulin-mediated odor adaptation by cAMP-gated channel subunits. Science *294*, 2176–2178.

Brown, R.L., Gramling, R., Bert, R.J., and Karpen, J.W. (1995). Cyclic GMP contact points within the 63-kDa subunit and a 240-kDa associated protein of retinal rod cGMP-activated channels. Biochemistry *34*, 8365–8370.

Chen, T.Y., and Yau, K.W. (1994). Direct modulation by Ca(2+)-calmodulin of cyclic nucleotide-activated channel of rat olfactory receptor neurons. Nature *368*, 545–548.

Chen, T.Y., Peng, Y.W., Dhallan, R.S., Ahamed, B., Reed, R.R., and Yau, K.W. (1993). A new subunit of the cyclic nucleotide-gated cation channel in retinal rods. Nature *362*, 764–767.

Chen, T.Y., Illing, M., Molday, L.L., Hsu, Y.T., Yau, K.W., and Molday, R.S. (1994). Subunit 2 (or beta) of retinal rod cGMP-gated cation channel is a component of the 240-kDa channel-associated protein and mediates Ca(2+)-calmodulin modulation. Proc. Natl. Acad. Sci. USA *91*, 11757–11761.

Clegg, R.M. (1992). Fluorescence resonance energy transfer and nucleic acids. Methods Enzymol. *211*, 353–388.

Dhallan, R.S., Yau, K.W., Schrader, K.A., and Reed, R.R. (1990). Primary structure and functional expression of a cyclic nucleotide-activated channel from olfactory neurons. Nature *347*, 184–187.

Erickson, M.G., Alseikhan, B.A., Peterson, B.Z., and Yue, D.T. (2001). Preassociation of calmodulin with voltage-gated Ca(2+) channels revealed by FRET in single living cells. Neuron *31*, 973–985.

Finn, J.T., Krautwurst, D., Schroeder, J.E., Chen, T.Y., Reed, R.R., and Yau, K.W. (1998). Functional co-assembly among subunits of cyclic-nucleotide-activated, nonselective cation channels, and across species from nematode to human. Biophys. J. *74*, 1333–1345.

Goulding, E.H., Ngai, J., Kramer, R.H., Colicos, S., Axel, R., Siegelbaum, S.A., and Chess, A. (1992). Molecular cloning and single-channel properties of the cyclic nucleotide-gated channel from catfish olfactory neurons. Neuron *8*, 45–58.

Hsu, Y.T., and Molday, R.S. (1993). Modulation of the cGMP-gated channel of rod photoreceptor cells by calmodulin. Nature *361*, 76–79.

Jan, L.Y., and Jan, Y.N. (1997). Cloned potassium channels from eukaryotes and prokaryotes. Annu. Rev. Neurosci. *20*, 91–123.

Kaupp, U.B., Niidome, T., Tanabe, T., Terada, S., Bonigk, W., Stuhmer, W., Cook, N.J., Kangawa, K., Matsuo, H., Hirose, T., et al. (1989). Primary structure and functional expression from complementary DNA of the rod photoreceptor cyclic GMP-gated channel. Nature *342*, 762–766.

Korschen, H.G., Illing, M., Seifert, R., Sesti, F., Williams, A., Gotzes, S., Colville, C., Muller, F., Dose, A., Godde, M., et al. (1995). A 240 kDa protein represents the complete beta subunit of the cyclic nucleotide-gated channel from rod photoreceptor. Neuron *15*, 627–636.

Kreienkamp, H.J., Maeda, R.K., Sine, S.M., and Taylor, P. (1995). Intersubunit contacts governing assembly of the mammalian nicotinic acetylcholine receptor. Neuron *14*, 635–644.

Kurahashi, T., and Menini, A. (1997). Mechanism of odorant adaptation in the olfactory receptor cell. Nature *385*, 725–729.

Li, M., Jan, Y.N., and Jan, L.Y. (1992). Specification of subunit assembly by the hydrophilic amino-terminal domain of the Shaker potassium channel. Science *257*, 1225–1230.

Liman, E.R., and Buck, L.B. (1994). A second subunit of the olfactory cyclic nucleotide-gated channel confers high sensitivity to cAMP. Neuron *13*, 611–621.

Liman, E.R., Tytgat, J., and Hess, P. (1992). Subunit stoichiometry of a mammalian K+ channel determined by construction of multimeric cDNAs. Neuron *9*, 861–871.

Liu, D.T., Tibbs, G.R., and Siegelbaum, S.A. (1996). Subunit stoichiometry of cyclic nucleotide-gated channels and effects of subunit order on channel function. Neuron *16*, 983–990.

Matulef, K., and Zagotta, W. (2002). Multimerization of the ligand binding domains of cyclic nucleotide-gated channels. Neuron *36*, 93–103.

Matulef, K., and Zagotta, W.N. (2003). Cyclic nucleotide-gated ion channels. Annu. Rev. Cell Dev. Biol. *19*, 23–44.

Miyawaki, A., Llopis, J., Heim, R., McCaffery, J.M., Adams, J.A., Ikura, M., and Tsien, R.Y. (1997). Fluorescent indicators for Ca^{2+} based on green fluorescent proteins and calmodulin. Nature *388*, 882–887.

Munger, S.D., Lane, A.P., Zhong, H., Leinders-Zufall, T., Yau, K.W., Zufall, F., and Reed, R.R. (2001). Central role of the CNGA4 channel subunit in Ca^{2+}-calmodulin-dependent odor adaptation. Science *294*, 2172–2175.

Patterson, G.H., Piston, D.W., and Barisas, B.G. (2000). Forster distances between green fluorescent protein pairs. Anal. Biochem. *284*, 438–440.

Robinson, R.B., and Siegelbaum, S.A. (2003). Hyperpolarization-activated cation currents: from molecules to physiological function. Annu. Rev. Physiol. *65*, 453–480.

Sautter, A., Zong, X., Hofmann, F., and Biel, M. (1998). An isoform of the rod photoreceptor cyclic nucleotide-gated channel beta subunit expressed in olfactory neurons. Proc. Natl. Acad. Sci. USA *95*, 4696–4701.

Selvin, P.R. (1995). Fluorescence resonance energy transfer. In Methods in Enzymology (San Diego: Academic Press), pp. 300–334.

Shammat, I.M., and Gordon, S.E. (1999). Stoichiometry and arrangement of subunits in rod cyclic nucleotide-gated channels. Neuron *23*, 809–819.

Shapiro, M.S., and Zagotta, W.N. (1998). Stoichiometry and arrange-

ment of heteromeric olfactory cyclic nucleotide-gated ion channels. Proc. Natl. Acad. Sci. USA *95*, 14546–14551.

Shapiro, M.S., and Zagotta, W.N. (2000). Structural basis for ligand selectivity of heteromeric olfactory cyclic nucleotide-gated channels. Biophys. J. *78*, 2307–2320.

Sine, S.M., Kreienkamp, H.J., Bren, N., Maeda, R., and Taylor, P. (1995). Molecular dissection of subunit interfaces in the acetylcholine receptor: identification of determinants of alpha-conotoxin M1 selectivity. Neuron *15*, 205–211.

Trudeau, M.C., and Zagotta, W.N. (2002a). An intersubunit interaction regulates trafficking of rod cyclic nucleotide-gated channels and is disrupted in an inherited form of blindness. Neuron *34*, 197–207.

Trudeau, M.C., and Zagotta, W.N. (2002b). Mechanism of calcium/calmodulin inhibition of rod cyclic nucleotide-gated channels. Proc. Natl. Acad. Sci. USA *99*, 8424–8429.

Trudeau, M.C., and Zagotta, W.N. (2003). Calcium/calmodulin modulation of olfactory and rod cyclic nucleotide-gated ion channels. J. Biol. Chem. *278*, 18705–18708.

Varnum, M.D., and Zagotta, W.N. (1996). Subunit interactions in the activation of cyclic nucleotide-gated ion channels. Biophys. J. *70*, 2667–2679.

Varnum, M.D., and Zagotta, W.N. (1997). Interdomain interactions underlying activation of cyclic nucleotide- gated channels. Science *278*, 110–113.

Weitz, D., Ficek, N., Kremmer, E., Bauer, P.J., and Kaupp, U.B. (2002). Subunit stoichiometry of the CNG channel of rod photoreceptors. Neuron *36*, 881–889.

Xu, J., Yu, W., Jan, Y.N., Jan, L.Y., and Li, M. (1995). Assembly of voltage-gated potassium channels. Conserved hydrophilic motifs determine subfamily-specific interactions between the alpha-subunits. J. Biol. Chem. *270*, 24761–24768.

Zagotta, W.N., Olivier, N.B., Black, K.D., Young, E.C., Olson, R., and Gouaux, E. (2003). Structural basis for modulation and agonist specificity of HCN pacemaker channels. Nature *425*, 200–205.

Zheng, J., and Zagotta, W.N. (2003). Patch-clamp fluorometry recording of conformational rearrangements of ion channels. Sci. STKE *2003*, PL7.

Zheng, J., Trudeau, M.C., and Zagotta, W.N. (2002). Rod cyclic nucleotide-gated channels have a stoichiometry of three CNGA1 subunits and one CNGB1 subunit. Neuron *36*, 891–896.

Zheng, J., Varnum, M.D., and Zagotta, W.N. (2003). Disruption of an intersubunit interaction underlies Ca^{2+}-calmodulin modulation of cyclic nucleotide-gated channels. J. Neurosci. *23*, 8167–8175.

Zhong, H., Lai, J., and Yau, K.W. (2003). Selective heteromeric assembly of cyclic nucleotide-gated channels. Proc. Natl. Acad. Sci. USA *100*, 5509–5513.

Zhong, H., Molday, L.L., Molday, R.S., and Yau, K.W. (2002). The heteromeric cyclic nucleotide-gated channel adopts a 3A:1B stoichiometry. Nature *420*, 193–198.

Zhou, L., and Siegelbaum, S.A. (2001). Rescue of non-expressing olfactory CNG channel (beta) subunits by replacement of its C-linker with subunit sequence. Biophys. J. *82*, 183a.

Zufall, F., and Munger, S.D. (2001). From odor and pheromone transduction to the organization of the sense of smell. Trends Neurosci. *24*, 191–193.